Hindawi
Advances in Civil Engineering
Volume 2022, Article ID 9040937, 12 pages
https://doi.org/10.1155/2022/9040937

Research Article

Study on the Cracking Mechanism of Arch Foot of CFST Tied Arch Bridge Based on Multiscale Numerical Simulation

Zeying Yang, Changhao Cai, Zhilin Qu, Chenghe Wang, and Yinglin Sun

School of Civil Engineering, Shandong University, Jinan, China

Correspondence should be addressed to Chenghe Wang; wangchenghe1999@163.com

Received 14 July 2022; Revised 5 September 2022; Accepted 11 October 2022; Published 7 November 2022

Academic Editor: Piotr Smarzewski

In order to study the causes of arch foot cracking, a multiscale numerical simulation method was used to establish the finite element model of Xizha Bridge during the construction stage of the Xiaoqing River restoration project in Jinan by using Midas Civil, and the internal forces under adverse conditions were extracted. On this basis, Abaqus was used to establish the local model of arch foot, and the plastic damage model parameters were introduced to conduct stress analysis. The results show that the anchorage stress of prestressed steel bundle is too high. On the one hand, the stress component produced by the bending of the prestressed steel bundle can squeeze the concrete inside the bending angle, and on the other hand, it will stretch the concrete outside the bending angle, resulting in concrete cracking. There is a tendency of relative displacement between arch rib and arch foot, and the interface surface of arch foot and arch rib is pulled by the displacement of arch rib, resulting in cracking. Arch foot inner bend produces a certain tensile stress, and if this place is not paid enough attention to, insufficient reinforcement will produce large cracks. Finally, it is suggested that concrete cracking can be avoided by arranging enough reinforcement bars under anchor and sealing reinforcement bars, encrypting steel mesh, arranging shear studs, and extending insertion depth.

1. Introduction

For concrete-filled steeltube tied arch bridges, cracking at the arch foot is more common. In this paper, taking the West Gate Bridge of the Xiaoqing River Rehabilitation Project in Jinan City as an example, Midas is used to analyze the completed bridge of the West Gate Bridge, and the local stress under different working conditions is obtained. The detailed modeling of the arch foot is carried out, and the local section stress is used as the external load. Abaqus finite element software is used to obtain the stress cloud diagram and plastic damage of the arch foot under different working conditions, and the causes of cracks are analyzed, and control measures are proposed. Most current research [1–5] shows that the structure of the arch foot joint is complex, which is prone to stress concentration and leads to concrete cracking. In this paper, the multiscale numerical simulation method is used to study the cracking cause and crack control of the arch foot.

2. Engineering Summary

Taking the Xizha Bridge of the Xiaoqing River restoration project as the engineering background in Shandong Province, China, the bridge is a concrete-filled steel tubular tied arch bridge with 90 m span and 17.2 m rise. The arch axis equation is $y = 4x\ (L-x)/L^2$, and the calculated rise-span ratio $f/L = 1/5$, $L = 86$ m, and $f = 17.2$ m. Arch rib adopts a dumbbell-shaped concrete filled steel tube, arch rib section height 260 mm, wall thickness 1.8 cm; C50 self-compacting shrinkage-compensating concrete is filled in steel tube, and C55 concrete is used in tie beam and cross beam. Both tie beams and end beams have prestressed steel beams to provide prestress, and two groups of prestressed tendons exist at the arch foot. The layout of the main bridge is shown in Figures 1 and 2.

3. Finite Element Analysis Model

Before the partial analysis of the arch foot, the stress condition of the arch foot should be calculated, that is, the

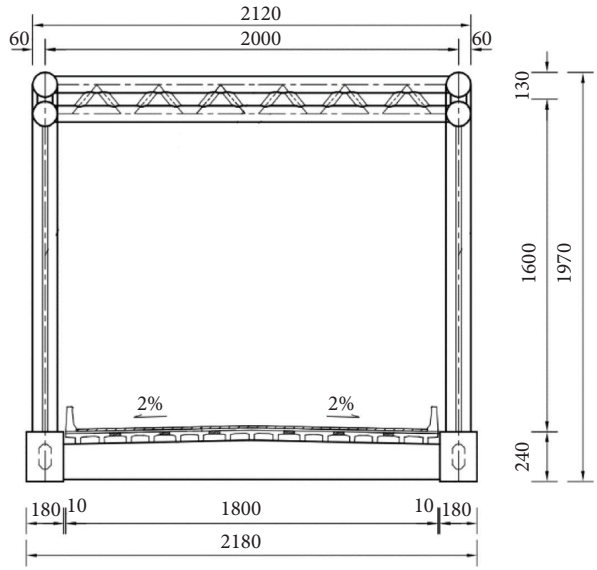

Figure 1: Cross-sectional diagrams of the analyzed bridge.

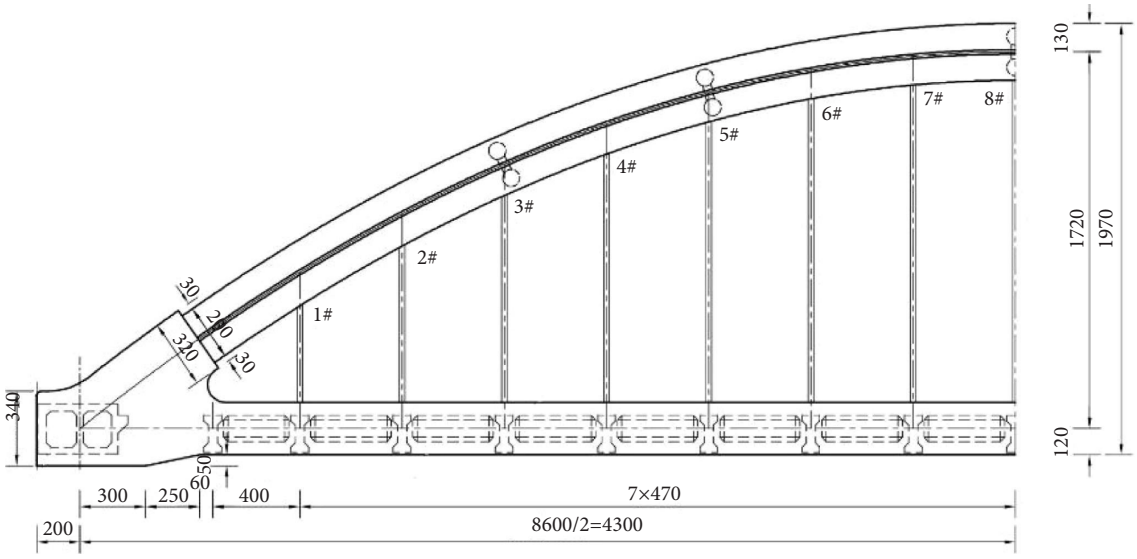

Figure 2: Overall view of the analyzed bridge (half arch).

internal force condition of the whole bridge at the truncation of the arch foot model [6]. Therefore, the finite element analysis of the whole bridge modeling was firstly carried out to obtain the stress state of the whole bridge under various working conditions, and then it was used as the external load input of the local modeling of the arch foot [7].

3.1. Finite Element Modeling of the Full Bridge. Finite element software Midas/Civil is used to establish the mechanical finite element model of Xizha Bridge in the construction stage. The suspender is simulated by the truss element (30 in total), and the beam element is used to simulate the beam part (887 in total). The arch rib section is constructed by the joint section. The spatial finite element model of Xizha Bridge is shown in the diagram. According to the actual construction process arrangement, a total of 18 construction stages are divided, and the specific division results are listed in Table 1. The Midas bridge model is shown in Figure 3.

3.2. Establishment of the Local Model of the Arch Foot

3.2.1. Model Assumptions

(1) The length of tie beam is 9000 mm, the length of end beam is 1850 mm, and the arch rib is extended by 800 mm from the arch foot surface.

(2) The influence of initial material defects and residual stresses on the overall force of the structure is not considered.

Table 1: Construction stage.

Working condition number	Construction stage	Construction days
1	Cast-in-place tie beam, cross beam, and arch foot	40
2	Partial prestress of first tension tie beam and cross beam	10
3	Installation of arch rib steel pipe and wind bracing	20
4	Concrete-filled steel tube under arch rib forms composites	7
5	Concrete-filled steel tube on arch rib forms a composite section	7
6	Arch rib participates in force	7
7	Installation of booms	10
8	First tension suspender $1^{\#}$, $4^{\#}$, $7^{\#}$	1
9	First tension suspender $2^{\#}$, $5^{\#}$, $8^{\#}$	1
10	First tension suspender $3^{\#}$, $6^{\#}$	1
11	Residual prestress of tension beam	1
12	Installation of road slab and pouring of wet joints	30
13	Prestressed residual tension beam	1
14	Bridge deck pavement and ancillary structures	30
15	Second tension suspender $1^{\#}$, $4^{\#}$, $7^{\#}$	1
16	Second tension suspender $2^{\#}$, $5^{\#}$, $8^{\#}$	1
17	Second tension suspender $3^{\#}$, $6^{\#}$	1
18	Bridge	10

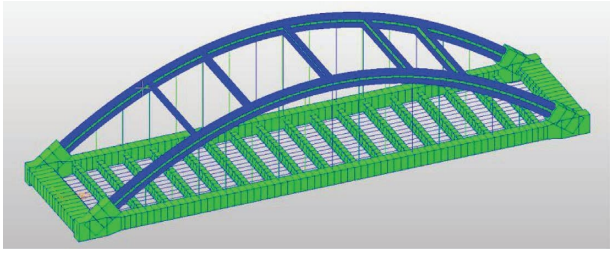

Figure 3: Midas civil bridge model.

(3) According to the Saint–Venant principle, the stress distribution at the section does not affect the distant stress distribution.

(4) Assuming that the reinforcement is always in the linear elastic stage, there is no plastic deformation.

(5) Creep of concrete is not considered.

3.2.2. Definition of the Model Material. The concrete grade is C55, the arch rib steel pipe is Q355, the steel bar adopts HRB400, the prestressed steel bundle adopts the low-relaxation steel strand conforming to the national standard of GB/T5224, $f_{pk} = 1860$ MPa, and the net protective layer is 3.5 cm. After calculation [8, 9], the parameters of C55 concrete plastic damage model are input into Abaqus.

(1) Simulation of concrete. In order to obtain the accurate results as far as possible, the structural mesh division technology is used in Abaqus by reasonable partition. The majority of concrete structures are C3D8R eight-node hexahedral elements, and the partial C3D6 wedge element and C3D10 tetrahedron element are used in local areas.

When defining material properties, in order to truly simulate the stress of concrete, it is necessary to determine the constitutive relation of concrete. The determination of uniaxial stress and strain relation of concrete is derived from the relevant formula in the concrete structure design code.

The stress-strain formula of uniaxial concrete in the code for design of concrete structures is as follows: the stress-strain formula of concrete under uniaxial tension:

$$\begin{aligned} \sigma &= (1 - d_t) E_c \varepsilon, \\ d_t &= 1 - \rho_t \left[1.2 - 0.2x^5\right], x < 1, \\ d_t &= 1 - \frac{\rho_t}{\alpha_t (x-1)^{1.7} + x}, x > 1, \\ x &= \frac{\varepsilon}{\varepsilon_{t,x}}, \rho_t = \frac{f_{t,r}}{E_c \varepsilon_{t,y}}. \end{aligned} \tag{1}$$

The stress-strain formula of concrete under uniaxial compression:

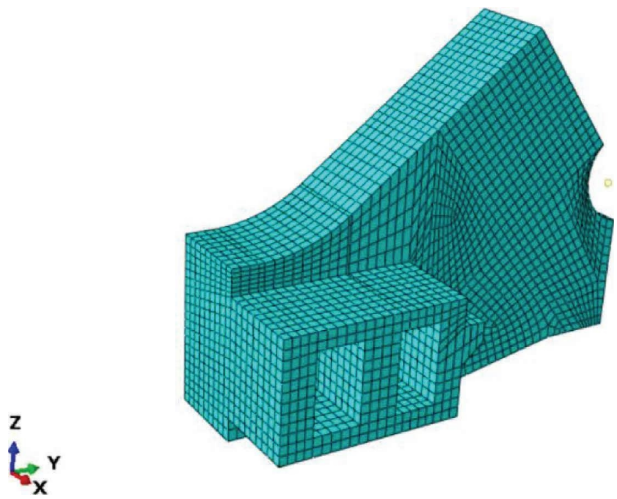

Figure 4: Grid division of concrete components.

$$\begin{aligned}
\sigma &= (1 - \mathrm{d}c)E_c\varepsilon,\\
\mathrm{d}_c &= 1 - \frac{\rho_c n}{x - 1 + x^n}, x \le 1,\\
\mathrm{d}_c &= 1 - \frac{\rho_c}{\alpha_c (x-1)^2 + x}, x > 1,\\
x &= \frac{\varepsilon}{\varepsilon c}, x^{\prime\rho_t} = \frac{f_{c,y}}{a}, n = \frac{E_c \varepsilon cr}{E_c \varepsilon cr - fcr}, a = E_c \varepsilon_{c,y},
\end{aligned} \tag{2}$$

where $f_{t,r}$ is the representative value of uniaxial tensile strength of concrete, MPa; d_t is damage evolution parameters of uniaxial concrete under tension; α_t is the parameters of descending section of uniaxial concrete under tensile state; $\varepsilon_{t,x}$ is the peak tensile strain of uniaxial concrete tensile strength; $f_{c,y}$ is the representative value of uniaxial compressive strength of concrete, MPa; $\varepsilon_{c,y}$ is the peak compressive strain of uniaxial concrete compressive strength; α_c is the parameters of descending section of uniaxial concrete under compression; d_c is the damage evolution parameters of uniaxial concrete under compression.

(2) Simulation of steel bars and steel pipes. Assuming that there is no plastic deformation between the steel bar and the steel tube, the steel bar element adopts the T3D2 three-dimensional two-node truss element, and the arch-ribbed steel tube element adopts the default S4R four-node surface shell element.

(3) Simulation of prestressed steel bundles. In order to apply prestress to the prestressed steel bundles by the cooling method, an expansion coefficient needs to be set, which is set to $1.2e-5$. The prestressed steel bundles use the same T3D2 three-dimensional two-node truss element as the steel mesh.

3.2.3. Model Grid Division. In order to obtain more accurate second-order accuracy, the concrete adopts the hexahedral-based meshing method. An arch rib steel pipe is modeled in the form of a shell, using the S4R element type. The T3D2 three-dimensional two-node truss element is used in steel bar and prestressed steel beam. The mesh division of the model is shown in Figure 4.

3.2.4. Interaction of the Arch Foot Model. The arch foot casting method is integrated casting, with the built-in area that can well simulate the relationship between the steel mesh and prestressed steel bundle and concrete, and there is no need to consider the anchorage situation alone. The reinforcement net and prestressed steel bundle are set as two embedded areas, respectively, and the concrete component is set as the main area, and the interaction relationship is defined through the function of the built-in area. The arch rib steel pipe, arch rib concrete, and arch foot concrete are bound together by binding constraints.

3.2.5. Boundary Condition. The truncated surface of the tie beam limits the longitudinal displacement and the angle of the transverse and vertical bridge, the truncated surface of the end beam limits the transverse displacement and the angle of the longitudinal and vertical bridge, the bottom of the arch foot limits the vertical displacement and the angle of the longitudinal and horizontal bridge, and the force at the end beam and the tie beam is replaced by the support reaction force.

3.2.6. Loading Case

(1) The internal force of each construction stage in the Midas Civil model is analyzed, and it is found that the internal force changes obviously under three working conditions. Therefore, the overall modeling analysis results of Midas Civil are extracted and imported into the local finite element model to analyze the three most unfavorable working conditions, as shown in Table 2.

(2) Temperature field

In this paper, the temperature drop method is used to simulate the prestress of the prestressed steel beam. Because the temperature of the prestressed steel beam element decreases, the temperature stress is produced, and the stress of the prestressed steel beam is simulated. The cooling amplitude is calculated by using the following formula:

$$\begin{aligned}
\sigma_{\mathrm{con}} &= \varepsilon_t E_t,\\
\varepsilon_t &= \alpha l \Delta t,
\end{aligned} \tag{3}$$

where σ_{con} is the tensile stress controlled by the steel bundle, which is 1395 MPa; ε_t is the strain of steel beam; E_t is the elastic modulus of the steel bundle, 195000; a_l is the linear expansion coefficient of the steel bundle, $1.2e-5$; Δt is the cooling range, which is -596.15°C.

Table 2: Loads under various working conditions.

Working condition number	Phase	Axial force (kN)	Bending moment (kN·m)
10	First tension suspender $3^{\#}$, $6^{\#}$	−11094.2	−2112.1
12	Installation of road slab and pouring of wet joints	−10387.4	−2157.9
17	Second tension suspender $3^{\#}$, $6^{\#}$	−22836.8	−838.1

4. Analysis of Finite Element Model Results

The calculation model is obtained by simplifying the model, partitioning the three-dimensional components and reasonable meshing. In this section, the stress analysis of steel and concrete is carried out, and the main tensile stress and main compressive stress nephogram are observed [10–12]. The region with the maximum stress under three working conditions is found, and the general stress distribution law is summarized. By observing the DAMAGEC field distribution diagram and DAMAGET field distribution diagram of concrete members, the regions with compressive plastic deformation and tensile plastic deformation are found out, and the targeted treatment measures for cracks in this region are put forward.

4.1. Analysis of Working Condition 10 Results

4.1.1. Analysis of Main Tensile Stress Nephogram of Arch Foot Concrete. In order to facilitate the observation of the stress cloud diagram of the key parts, the larger principal compressive stress and the principal compressive stress caused by the prestressed anchorage are hidden in the analysis, and the elements with excessive stress caused by the anchorage are removed. As shown in Figure 5, it can be found that in working condition 10, the maximum principal tensile stress occurs in three places: the first is the central position of the lower part of the arch foot, the second is the interface between the arch rib insertion arch foot and the arch foot concrete, and the third is the upper edge of the arch foot.

For the large main tensile stress in the second place, referring to the engineering drawings, it is found that, as shown in Figure 6, the prestressed steel bundle in the lower part has a large vertical bending, and this vertical bending causes a part of the prestressed component to form a vertical bending. The resultant force below pulls the concrete, so the arch foot is easy to form a large main tensile stress in the place where the prestressed steel bundle is bent, resulting in possible cracks.

For the second place, the great principal tensile stress is due to the huge axial force of the arch rib, which leads to the relative inward sliding trend of the concrete on the surface, and then produces a huge tensile stress to maintain the deformation coordination, which is an important reason for the concrete crack on the interface surface of the arch rib and concrete.

4.1.2. Cloud Analysis of Main Compressive Stress of Arch Foot Concrete. It is found that there is a larger principal compressive stress in the blue-green region shown in Figure 7, which is similar to the larger principal tensile stress in the second place in this section. The reason for the larger principal compressive stress of concrete in this area is the same as that of the larger principal tensile stress of some concrete in the previous section, which is caused by the bending of prestressed steel beams.

4.1.3. Output Analysis of Plastic Damage of Arch Foot Concrete. It can be seen from Figure 8 that the compressive plastic damage of concrete mainly occurs at the anchorage of prestressed steel beam.

From Figure 9, it can be seen that the tensile plastic damage of concrete occurs in the place where the main tensile stress mentioned previously is larger.

The previous results show that although the main compressive stress and main tensile stress are relatively large in concrete, the plastic damage is mainly tensile plastic damage, and the possibility of cracks in arch foot caused by tensile cracking is much greater than that caused by crushing.

4.2. Analysis of Working Condition 12 Results. Figures 10 and 11 show the cloud diagram of principal tensile stress and compressive stress at the twelve arch feet without anchorage. By observing the calculation results of condition 12, it is found that the cloud images of each stress are similar to those of condition 10, which is because the load of condition 12 is similar to that of condition 18, and the relative prestress is relatively small. At the interface between the arch rib and the arch foot, the tensile stress of condition 12 is greater than that of condition 10, which indicates that the maximum principal tensile stress is positively correlated with the axial force of the arch rib.

4.3. Analysis of Working Condition 17 Results

4.3.1. Analysis of Main Tensile Stress Nephogram of Arch Foot Concrete. Figure 12 shows the cloud diagram of main tensile stress at the anchorage point of arch foot in working condition 17. In working condition 17, the main tensile stress at the upper edge of the inner bending of the arch foot does not increase with the increase of the arch rib axial force, but it becomes smaller than that in working condition 10 and working condition 12, indicating that the main tensile stress here is not determined by the arch rib axial force. By comparing the bending moments of arch ribs under three working conditions, it is found that the bending moment of working condition 12 is the largest, and that of working condition 10 and that of working condition 17 are the smallest. The order of principal tensile stress here is also consistent with this. Therefore, it is not difficult to

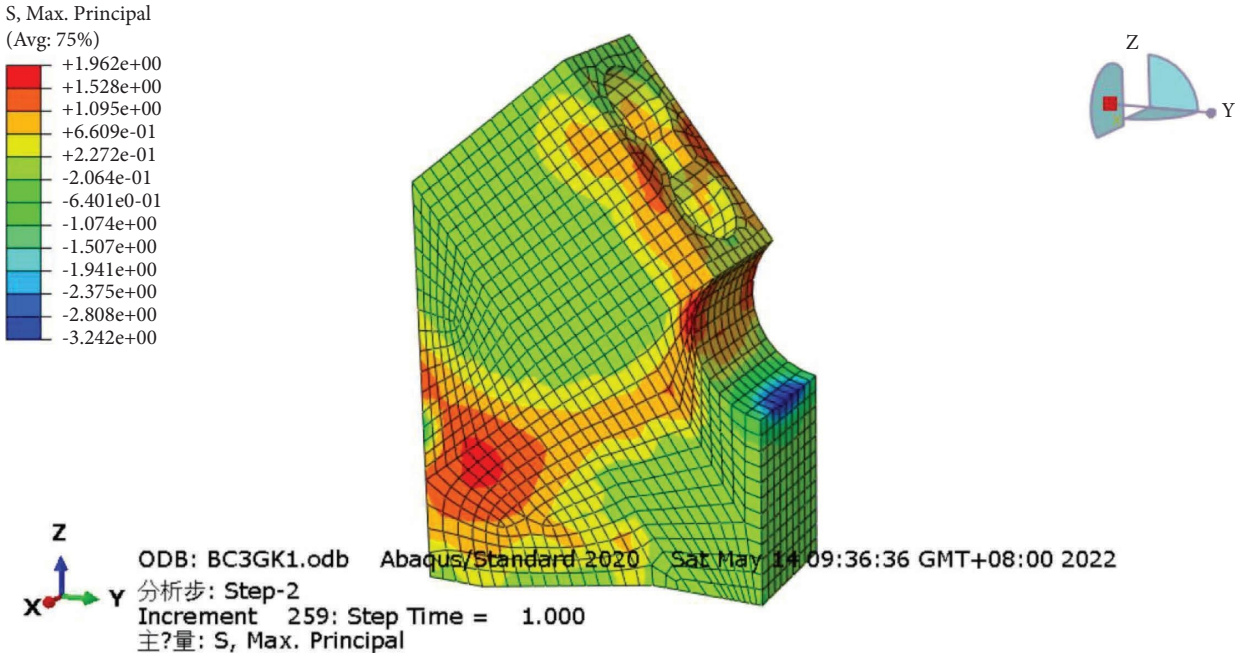

Figure 5: Cloud chart of the principal tensile stress of the arch foot without anchorage of condition 10.

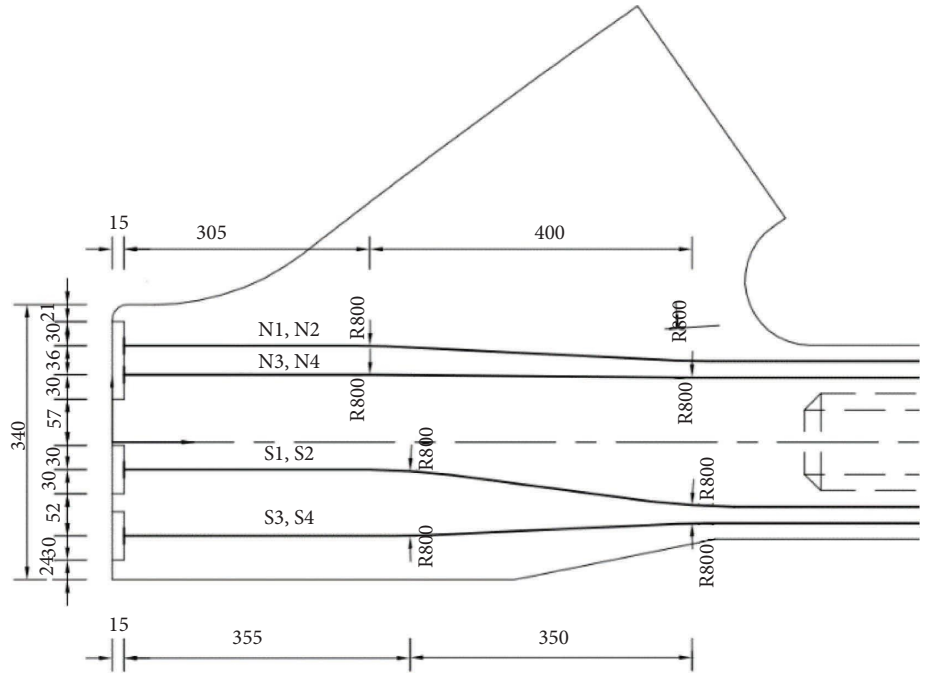

Figure 6: Bending diagram of prestressed steel wires at arch foot.

find that the main tensile stress here comes from the bending moment brought by the arch rib, which leads to the tensile side here.

4.3.2. Cloud Analysis of Main Compressive Stress of Arch Foot Concrete. Figure 13 shows the cloud diagram of the main compressive stress at the arch foot without anchorage in working condition 17. The maximum principal compressive stress of working condition 17 is smaller than that of working condition 10 and working condition 12, which is due to the greater axial force of arch rib that brings greater horizontal force and reduces the compressive stress of concrete in tie beam direction caused by prestress. But at the same time, the prestressed steel beam has to bear greater stress, which brings greater tensile and compressive stress to the anchorage end concrete.

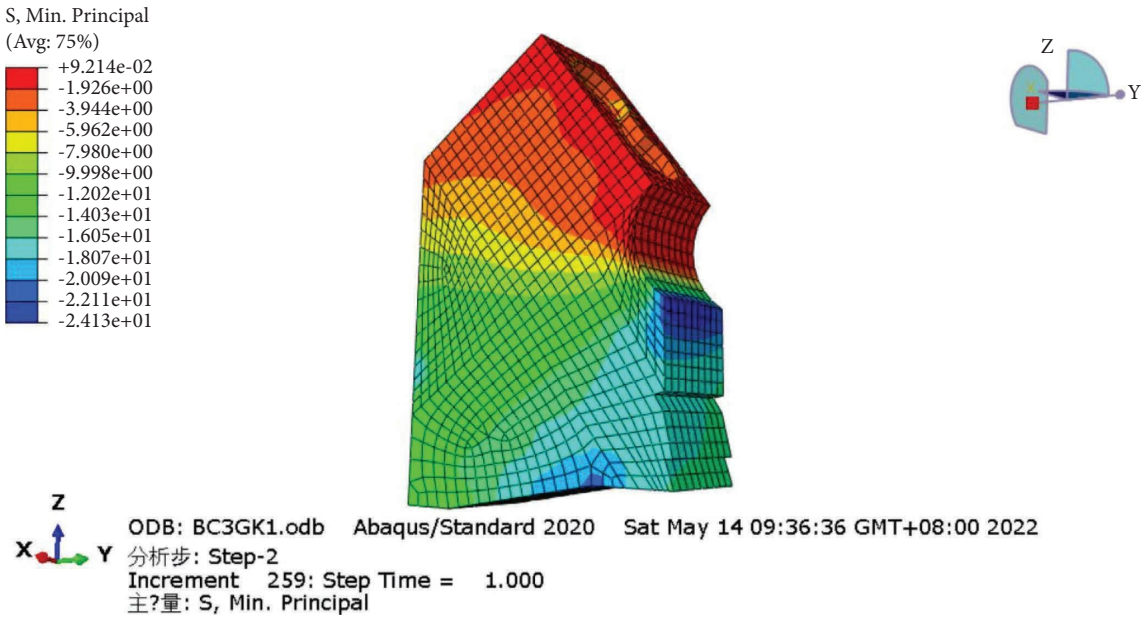

Figure 7: Cloud chart of the principal compressive stress of arch foot without anchorage of condition 10.

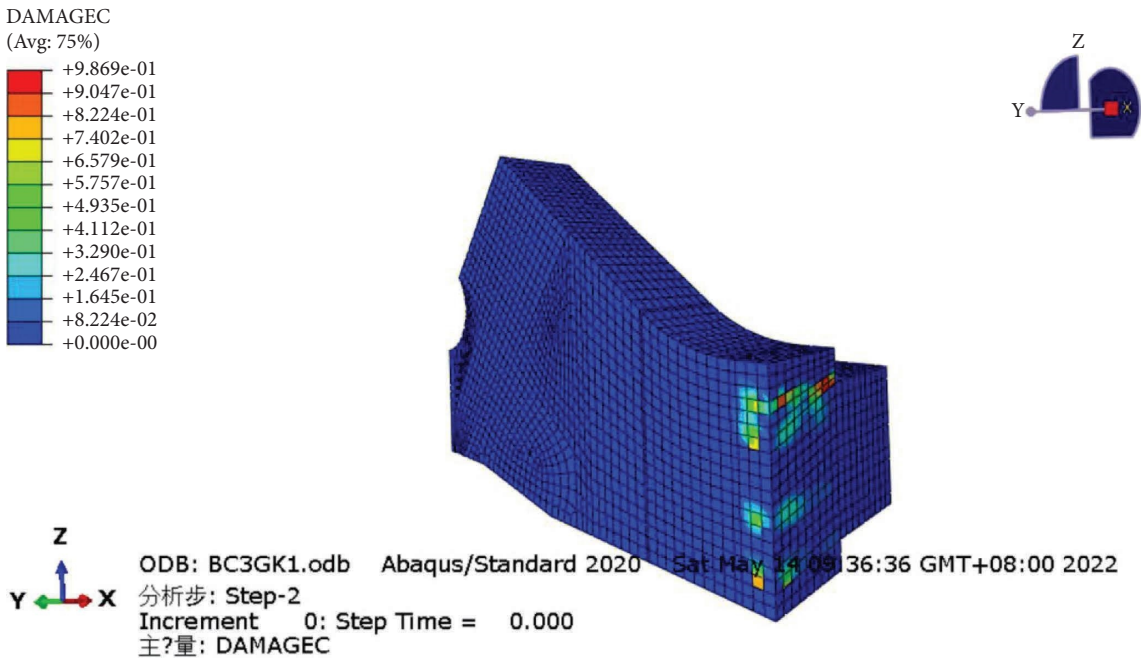

Figure 8: Cloud chart of concrete compression plastic damage of condition 10.

4.3.3. Output Analysis of Plastic Damage of Arch Foot Concrete. Figures 14 and 15 show the plastic damage cloud of concrete. The plastic damage position of condition 17 has no change compared with condition 10 and condition 12, but it has a certain development in the anchorage end of prestressed steel beam, which confirms the analysis of 3.4.2.

5. Causes and Countermeasures

5.1. Causes of Cracks

(1) The anchorage end stress of the prestressed steel bundle is too large. If the measures such as anchor reinforcement and anchor reinforcement are not in place

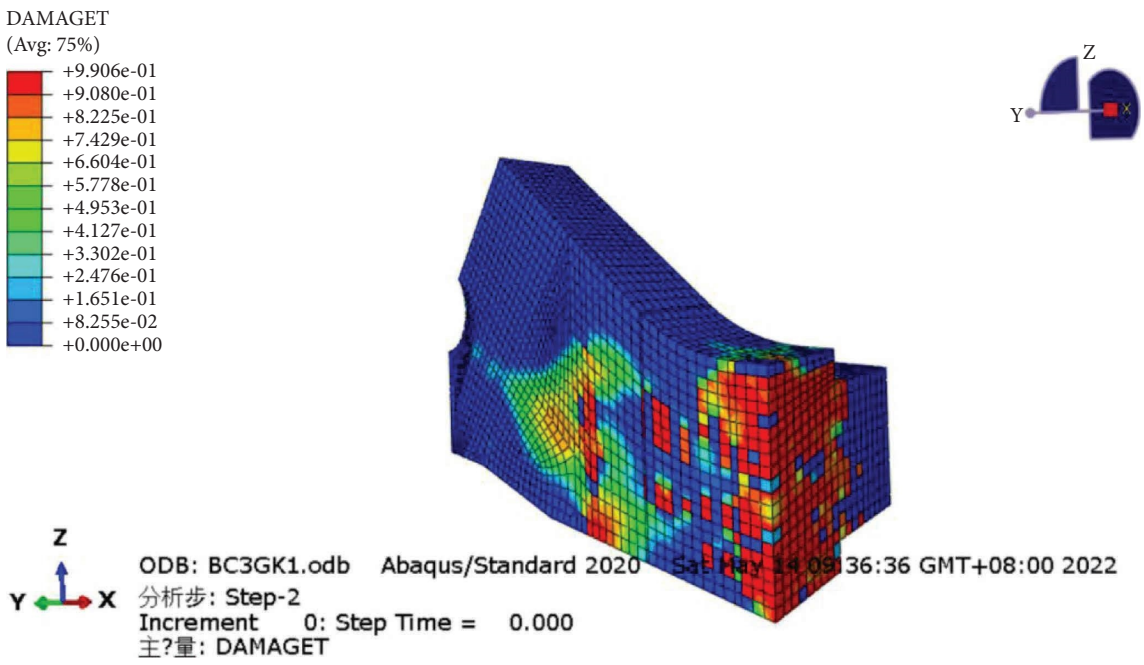

Figure 9: Cloud chart of tensile plastic damage of concrete of condition 10.

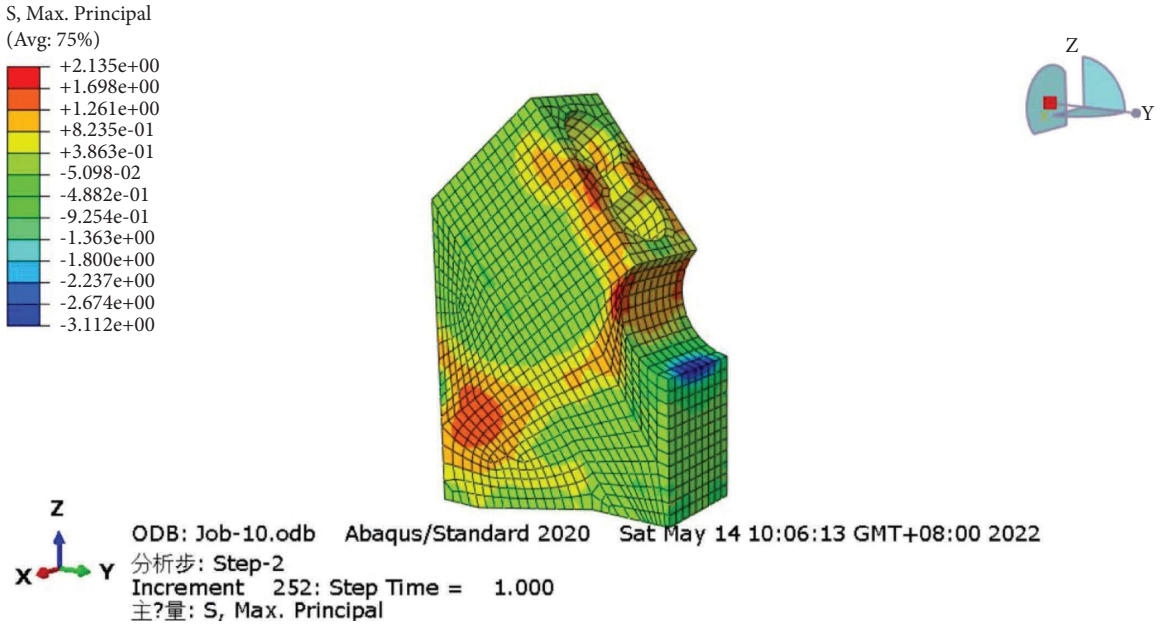

Figure 10: Cloud chart of the principal tensile stress of the arch foot without anchorage of condition 12.

enough, the huge stress of the prestressed steel bundle at the end will be borne by the concrete. Whether under tension or compression, it is far beyond the ultimate bearing capacity of the concrete, which is the most significant factor of concrete cracking at the arch foot.

(2) The bending of prestressed steel beam. Since the tensile stress of the prestressed steel beam is very large, only a small angle is needed to show a huge stress component. On the one hand, this stress component can squeeze the concrete inside the bending angle, and on the other hand, it will stretch the concrete outside the bending angle, resulting in concrete cracking.

(3) The relative displacement trend of arch rib and arch foot. The large axial force of the arch rib leads to the trend of more in-depth arch foot displacement. The interface between the arch foot and the arch rib is pulled by the displacement of the arch rib, which leads to cracking.

(4) Tension caused by the arch rib bending moment. Although the arch rib bending moment of tied arch

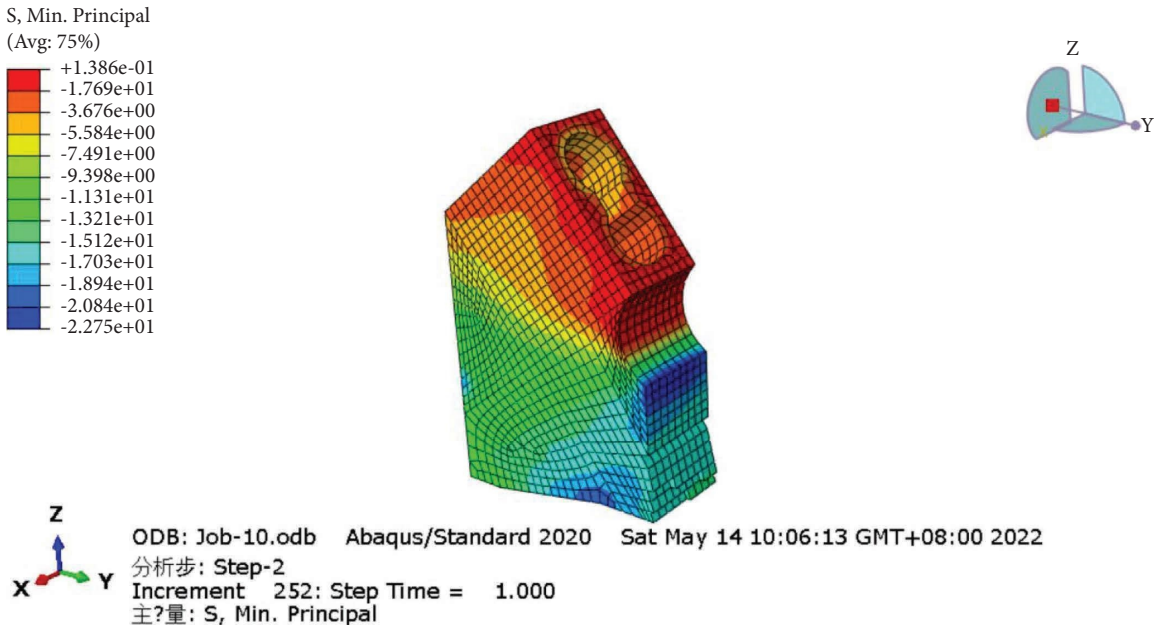

Figure 11: Cloud chart of the principal compressive stress of the arch foot without anchorage of condition 12.

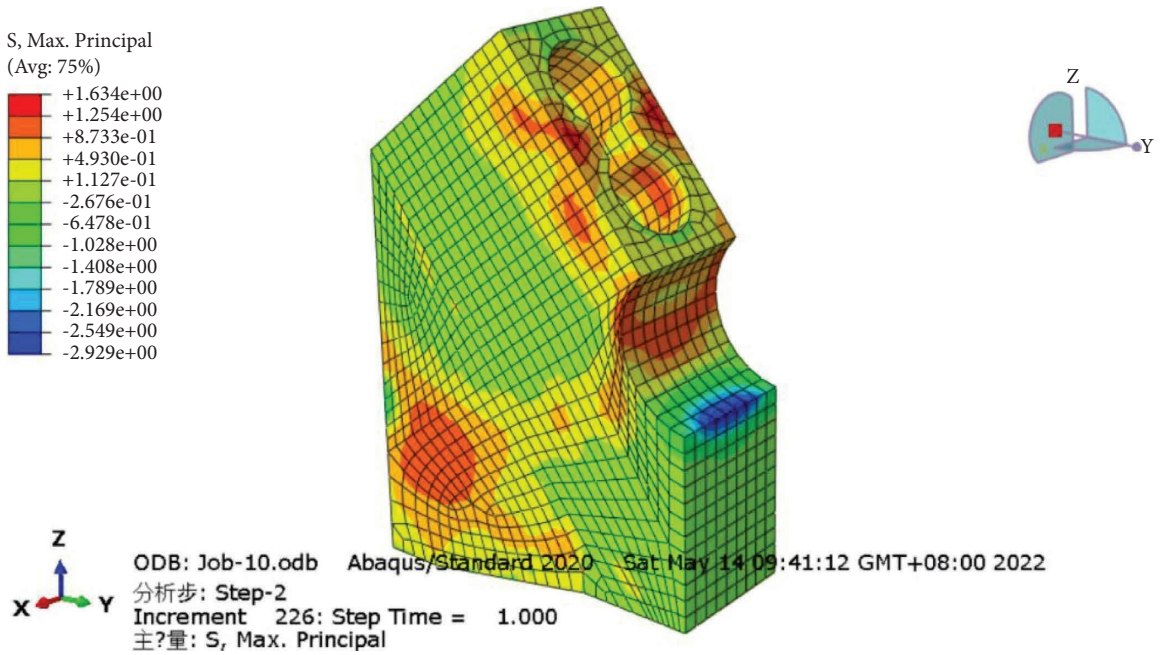

Figure 12: Cloud chart of the principal tensile stress of arch foot without anchorage of condition 17.

bridge is very small, certain tensile stress can still be generated at the internal bending of arch foot, and it has slightly exceeded the tensile limit of C55 concrete. If we do not pay enough attention to this place and lack of reinforcement, it is possible to produce large cracks.

5.2. Countermeasures

(1) Take enough anchorage measures at the anchorage end of the prestressed steel beam. Avoid the prestressed steel beam end of the traction force concentrated on a small area of concrete. Adequate anchor reinforcement and sealing reinforcement are arranged to improve the overall stiffness of reinforced concrete here to ensure that it does not cause excessive deformation due to prestressed steel bundles.

(2) Prestressed steel beam in the weak parts as smooth as possible. Avoid tearing concrete due to the large stress component of prestressed steel beam bending. If the bending angle is as small as possible and the

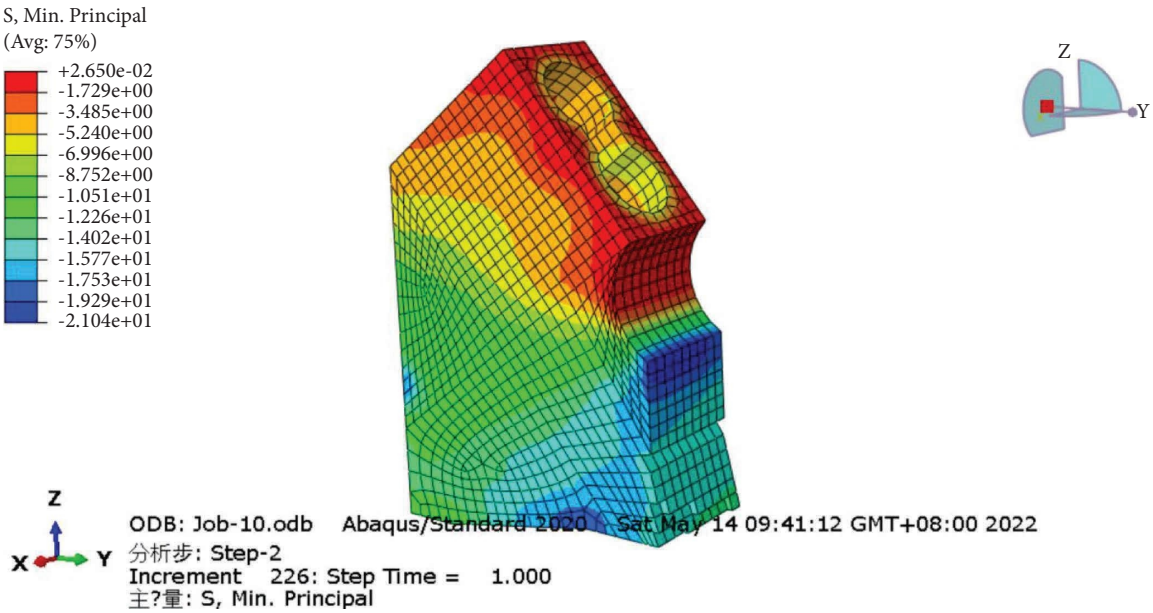

Figure 13: Cloud chart of the principal compressive stress of arch foot without anchorage of condition 17.

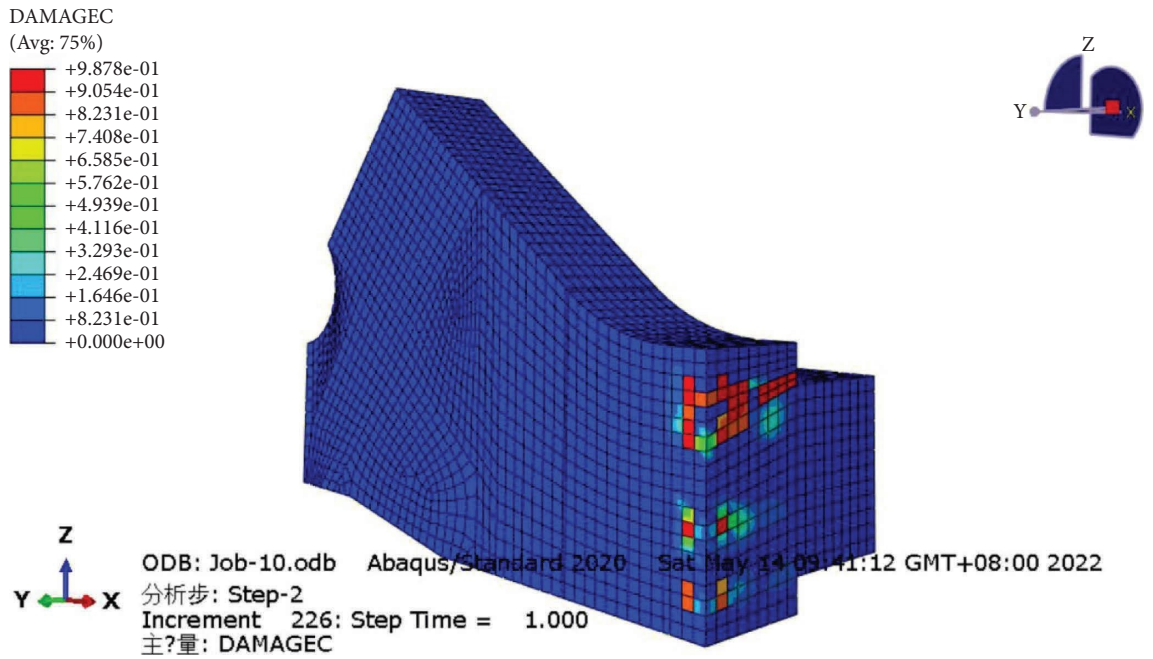

Figure 14: Cloud chart of concrete compression plastic damage of condition 17.

curve is as smooth as possible due to the change of section, the stress component is not concentrated on a small piece of concrete. In the bending place, attention should be paid to the arrangement of encrypted steel mesh to improve the overall stiffness of reinforced concrete.

(3) Pay attention to the section tension zone caused by the arch rib bending moment. The bending moment of arch rib is small and easy to be ignored, but the maximum principal tensile stress in the tensile zone generated by the bending moment of the arch rib has exceeded the ultimate tensile strength of C55 concrete, and it has cracked according to the first strength theory. In places where tension may be caused by the bending moment, reinforcement should also be reasonably arranged to avoid cracking.

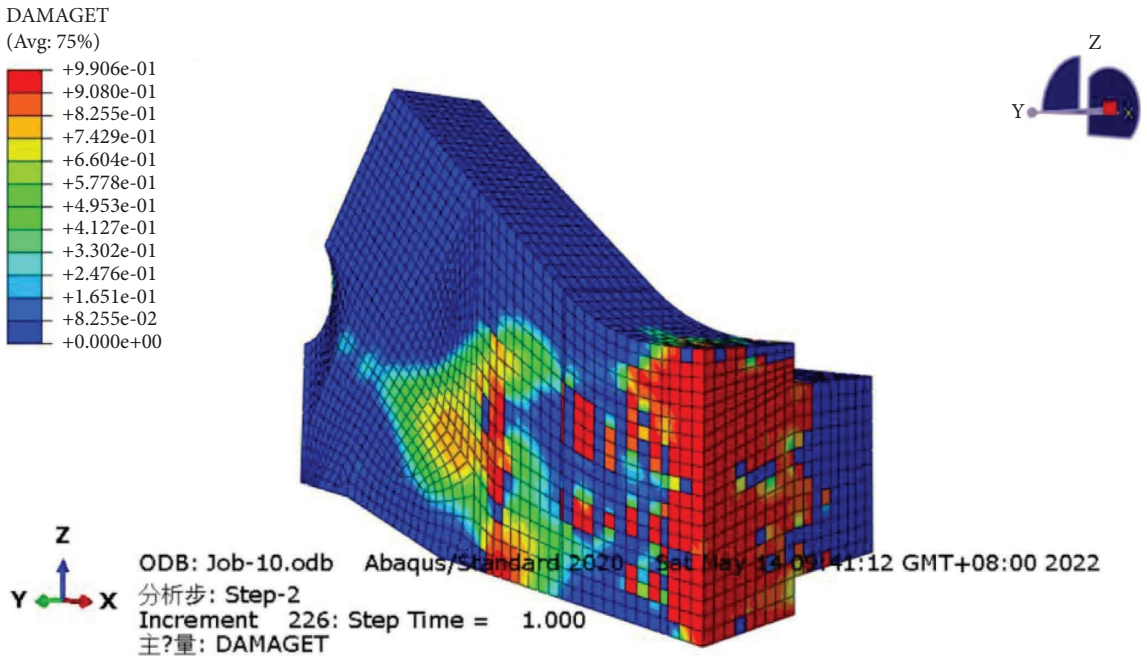

Figure 15: Cloud chart of concrete tensile plastic damage of condition 17.

6. Conclusion

Combined with Midas Civil and Abaqus software, through multiscale numerical simulation analysis, according to the stress cloud diagram, the local stress of the arch foot caused by prestress and external load is shown. The causes of arch foot cracking of concrete filled steel tube arch bridge are studied, including

(1) Prestressed steel anchor end stress is too large which will lead to concrete at the end of the bear huge stress

(2) The stress component caused by the bending of the prestressed steel strand makes the concrete to be stretched and squeezed, resulting in concrete cracking

(3) The junction of the arch foot and arch rib is cracked due to the relative displacement trend

(4) There is a certain tensile stress at the inner bending of the arch foot, which will produce large cracks

On this basis, in the design and construction, we should pay attention to (1) arranging enough anchor reinforcement and anchor reinforcement; (2) adjusting the prestressed steel bending angle; (3) arranging steel bars to avoid tensile stress caused by the bending moment of the arch rib.

Data Availability

The data that support the findings of this study are available from the corresponding author upon reasonable request.

Conflicts of Interest

The authors declare that they have no conflicts of interest.

Acknowledgments

The Transport Science and Technology Plan of Shandong Province, China 2021B85.

References

[1] L. Ming and K. Wu, "Cause analysis and prevention measures of arch abutment cracks in concrete filled steel tubular tied arch bridge," *Highway Traffic Science and Technology (Application Technology Version)*, vol. 12, no. 12, pp. 150–152, 2016.

[2] J. Shi, "Local stress analysis of arch foot of a railway trough girder arch bridge," *Engineering Construction and Design*, vol. 14, pp. 66–68, 2021.

[3] F. Wang, Li Liang, and Y. Li, "Local stress finite element analysis of arch foot of tied arch bridge," *Journal of Shenyang Jianzhu University (Natural Science Edition)*, vol. 2, pp. 281–285, 2011.

[4] W. Tian, "Arch foot design and local stress analysis of lhasa river bridge," *Bridge Construction*, vol. 5, pp. 20–23, 2005.

[5] Z. Zheng, Y. Xu, and B. Chen, "Local stress analysis of the consolidation point of the arch pier of Shenzhen North railway station bridge," *Journal of China Highway*, vol. 2, pp. 71–74, 2000.

[6] X. Liu, "Research on local stress of arch foot of highway network suspender arch bridge," *Urban Road and Bridge and Flood Control*, vol. 11, pp. 63–65, 2021.

[7] J. Mao, "Study on local stress of arch-beam joint section of long-span steel box tied arch bridge," *Bridge and Tunnel Engineering*, vol. 11, pp. 139–142, 2021.

[8] T. Zhang, "Numerical simulation of typical concrete models under monotonic and cyclic loading," *Kunming University of Technology*, 2020.

[9] X. Peng, "Parameter Analysis of concrete Damage Plasticity Model," *Journal of Suzhou University of Science and Technology*, vol. 26, pp. 43–46, 2010.

[10] J. Chen, *Local Stress Analysis of Arch Foot of Long-Span Continuous Beam-Arch Composite Bridge*, Lanzhou Jiaotong University, Gan Su Sheng, Lan Zhou, 2013.
[11] K. Zheng, *Long-span Railway Continuous Beam-Arch Composite Bridge Overall Analysis and Arch Foot Stress Research*, Southwest Jiaotong University, Si Chuan Sheng, 2018.
[12] I. Yellow, *Stress Optimization Analysis of Steel Beam and anchorage Zone of Continuous Beam Bridge Based on Numerical Analysis*, Changchun Institute of Engineering, Changchun, 2021.